# Characterization of surface impedance of vibro-acoustic subdomains with experimental measurements

M. Grialou, Nicolas Totaro, J.-L. Guyader, A. Bocquillet

Version of Record: https://www.sciencedirect.com/science/article/pii/S0022460X19304389
Manuscript_2c28d0f73ff4023c2465f93c76cda986

# Characterization of surface impedance of vibro-acoustic subdomains with experimental measurements

M. Grialou[a,b], N. Totaro[a,1], J.-L. Guyader[a], A. Bocquillet[b]

[a] *Univ Lyon, INSA-Lyon, Laboratoire Vibrations Acoustique, F-69621 Villeurbanne, France*

[b] *BMW Group, Knorrstrasse 147, 80788 Munich, Germany*

## Abstract

In substructuring approaches in the field of acoustics, subdomains are mostly characterized by impedance or mobility at their interfaces with other subdomains. This allows handling large systems broken down into smaller, easier to solve subdomains and reaching higher frequency ranges. When a subdomain is characterized by experiments, the impedances are often measured on a dedicated setup aimed at uncoupling the subdomain from the other subdomains. This is often hardly feasible and the setup is insufficiently versatile. In the present article, an inverse method is proposed to experimentally identify the surface impedance of a passive acoustic (or vibro-acoustic) subdomain by means of measurements performed on the whole coupled system. An analytical study illustrates the ability of the approach to identify the impedance matrix of a passive subdomain with accuracy. Nevertheless, as many inverse methods, the system of equations to solve is ill-conditioned. To address this issue, an original approach for tackling the ill-posedness of the problem is proposed. It is based on a statistical analysis of different versions of the matrix to identify. Finally, an experimental validation of the proposed approach is detailed and shows a good agreement when comparing to an available analytical solution.

*Keywords:* Surface impedance, Patch Transfer Functions method, inverse characterization, median

[1]Corresponding author. Tel.: + 33472438082. E-mail address: nicolas.totaro@insa-lyon.fr

## 1. Introduction

In the field of noise vibration and harshness (NVH), dynamic substructuring is often used to solve large problems or to reach higher frequencies. D. de Klerk listed [1] several advantages of a component-wise vision over a global method where the full system is handled as a whole:

- Handling large structures. Handling a large and complex system as a whole might be problematic due, for example, to the huge number of degrees of freedom when the system is modeled by a finite element model.

- Modification of a part of the structure without recomputing the response of the whole system. In substructuring approaches, there is no need to recompute the response of subdomains that are not affected by a structural modification, considerably reducing computation time and the pre-design process.

- Coupling different approaches. Each subdomain can be modeled separately by the most appropriate method. This can guarantee confidentiality when combining substructures from different actors.

Historically, in the late 19th century the impedance and mobility methods were developed to manage the complexity of electrical networks [2]. At the beginning of the 20th century, the discovery of the mechanical-electrical analogy allowed adapting this framework in the field of NVH [3].
More recently, Cacciolati and Guyader adapted the impedance and mobility method to the needs of acoustics and vibro-acoustics [4]. The continuous coupling interface was divided into elementary surfaces called patches defining the basis of the "patch-mobility method". The method has been further developed and applied to different cases [5–7]. Maxit proposed an alternative method, based on "patch-impedance" [8] which was further developed by Ouisse *et. al.* [9].
In the framework of this so-called PTF (Patch Transfer Functions) method, a coupled system can be considered as several subdomains connected by sets of patches. In terms of methodology, large and complex problems can be broken down into simpler sub-problems. Various methods can then be applied to compute the vibro-acoustical behavior of each subdomain. Once these

individual vibro-acoustical responses have been obtained, the response of the fully coupled system can be predicted by reassembling the subdomains using continuity relations.
The matrices of condensed impedances involved in a PTF model are much smaller than a full FEM or BEM model of the whole system. Consequently, the vibro-acoustical response of the system can be predicted with less computational effort. Therefore, the method is perfectly suitable for running an optimization algorithm [10].
The term "hybrid model" is used when different methods are used to obtain the PTF of the subdomains of a complex system. An example can be found in "A Combined Computational-Experimental Approach for Modelling Coupled Vibro-Acoustic Problems" experimented by Rejlek *et. al.* [11].
In some situations, an experimental characterization of the PTF is preferred over computation with a numerical model. This choice is generally due to the difficulty of obtaining a reliable model of complex subdomains (mainly in the case of vibro-acoustic subdomains like a car compartment with trim). Indeed, for some cases, the experimental identification of the patch impedance is the only means of introducing a subdomain in a vibro-acoustic computation.
A direct measurement of the PTF of a subdomain was proposed by Du [12]. In this case, the system was physically isolated with an interface discretized into mobile pistons (equivalent to patches). Each piston (patch) was activated separately to measure the blocked pressure on each patch. A similar method was proposed by Veronesi [13] to characterize poroelastic liners. In both cases, the impedance measurement was performed on an uncoupled subdomain, that is to say, in a particular setup. In the present work, an inverse method is proposed for the identification of the patch impedances of a passive subdomain. The originalities of this work are twofold and comprise:

- an experimental identification of the patch impedance using acoustic measurements on the whole system without uncoupling the subdomain being characterized from it.

- a regularization process based on the median of a set of identified matrices.

The theoretical basis of this approach is first described using an illustrative example and the proof of concept is given for a simple numerical test

case. Finally, an experimental validation is proposed to demonstrate that the present approach can be relevant in real measurement conditions.

## 2. Vibroacoustic solving using the Patch Transfer Functions (PTF) method

### *2.1. System under study*

As an illustrative example, let us consider a closed cavity $\Omega$ filled with air and delimited by a rigid surface $\partial\Omega$ presented in Fig. 1. A point source $S$ is active in the cavity. The acoustic pressure at point $M$ is denoted $p(M)$. According to the PTF method [9, 10], the whole domain $\Omega$ can be arbitrarily divided into coupled subdomains. In the case of Fig. 1, the acoustic cavity $\Omega$ is divided into two subvolumes $\Omega_{\mathrm{A}}$ and $\Omega_{\mathrm{B}}$ ($\Omega = \Omega_{\mathrm{A}} \cup \Omega_{\mathrm{B}}$) delimited by surfaces $\partial\Omega_{\mathrm{A}} \cup \Gamma$ and $\partial\Omega_{\mathrm{B}} \cup \Gamma$ ($\partial\Omega = \partial\Omega_{\mathrm{A}} \cup \partial\Omega_{\mathrm{B}}$), respectively. The coupling surface $\Gamma$ is arbitrary and has no physical meaning. This surface is divided into $N$ elementary surfaces called *patches*.

### *2.2. Coupling pressures and coupling acoustic velocities*

In this section, a summary of equations derived in [9] and [14] is presented for sake of clarity. Considering subdomain A, the averaged pressure (defined as $\frac{1}{\Gamma_i}\int_{\Gamma_i} p(M)\ \mathrm{d}M$) on the surface $\Gamma_i$ of patch $i$ is

$$p_i^{\mathrm{A}} = \tilde{p}_i^{\mathrm{A}} + \sum_{j=1}^{N} Z_{ij}^{\mathrm{A}} V_j^{\mathrm{A}} \tag{1}$$

and for all the $N$ patches

$$\mathbf{p}^{\mathrm{A}} = \tilde{\mathbf{p}}^{\mathrm{A}} + \mathbf{Z}^{\mathrm{A}}\mathbf{v}^{\mathrm{A}} \tag{2}$$

where $\tilde{\mathbf{p}}^{\mathrm{A}}$ is the direct pressure field due to the source $S$ and $\mathbf{Z}^{\mathrm{A}}\mathbf{v}^{\mathrm{A}}$ is the contribution of the acoustic velocities of the $N$ patches. $\mathbf{Z}^{\mathrm{A}}$ is the $N \times N$ acoustic impedance matrix of subdomain A.
Considering subdomain B, the averaged pressure on patch $i$ is

$$p_i^{\mathrm{B}} = \sum_{j=1}^{N} Z_{ij}^{\mathrm{B}} V_j^{\mathrm{B}} \tag{3}$$

and for all the $N$ patches

$$\mathbf{p}^{\mathrm{B}} = \mathbf{Z}^{\mathrm{B}}\mathbf{v}^{\mathrm{B}} \tag{4}$$

where $\mathbf{Z}^{\mathrm{B}}\mathbf{v}^{\mathrm{B}}$ is the contribution of the acoustic velocities of the N patches (no source is acting in this subdomain). $\mathbf{Z}^{\mathrm{B}}$ is the $N \times N$ acoustic impedance matrix of subdomain B.
When the two subdomains A and B are coupled, the following coupling conditions occur

$$\mathbf{p}^{\mathrm{A}} = \mathbf{p}^{\mathrm{B}} = \mathbf{p}^{\mathrm{coupl}} \tag{5}$$

and

$$-\mathbf{v}^{\mathrm{A}} = \mathbf{v}^{\mathrm{B}} = \mathbf{v}^{\mathrm{coupl}}, \tag{6}$$

according to the outward normals of the subdomains and where $\mathbf{p}^{\mathrm{coupl}}$ and $\mathbf{v}^{\mathrm{coupl}}$ are the coupling pressures and the coupling acoustic velocities.
The coupling acoustic velocities are deduced from Eqs. (2), (4) and (5) as

$$\mathbf{v}^{\mathrm{coupl}} = (\mathbf{Z}^{\mathrm{A}} + \mathbf{Z}^{\mathrm{B}})^{-1}\tilde{\mathbf{p}}^{\mathrm{A}} \tag{7}$$

and the coupling pressures are obtained from either Eq. (2) or Eq. (4) and coupling conditions (5) and (6). From Eq. (4), we obtain:

$$\mathbf{p}^{\mathrm{coupl}} = \mathbf{Z}^{\mathrm{B}}\mathbf{v}^{\mathrm{coupl}}. \tag{8}$$

The acoustic velocities are the primary unknowns of the PTF method. Once they are determined, the pressure can be computed at any point of the whole domain $\Omega$, as illustrated in [9].

*2.3. Subdomain characterization*

Let us consider that the coupling pressures $\mathbf{p}^{\mathrm{coupl}}$ and the coupling acoustic velocities $\mathbf{v}^{\mathrm{coupl}}$ can be experimentally measured for a particular position of the source S. In this case, Eq. (8) still occurs. If another experiment (a $k$-th experiment) is performed with another position of the source S, the coupling pressures and the coupling acoustic velocities are changed to $\mathbf{p}_k^{\mathrm{coupl}}$ and $\mathbf{v}_k^{\mathrm{coupl}}$ and Eq. (8) writes

$$\mathbf{p}_k^{\mathrm{coupl}} = \mathbf{Z}^{\mathrm{B}}\mathbf{v}_k^{\mathrm{coupl}}. \tag{9}$$

It should be emphasized that in Eq.(9), the $\mathbf{Z}^{\mathrm{B}}$ matrix does not change as it is independent of the source position. Thus, if $N$ experiments are performed, the $N$ vectors $\mathbf{p}_k^{\mathrm{coupl}}$ and $\mathbf{v}_k^{\mathrm{coupl}}$ can be stacked in two matrices $\mathbf{P}^{\mathrm{c}}$ and $\mathbf{V}^{\mathrm{c}}$, each of them having dimensions $N \times N$. This gives:

$$\mathbf{P}^{\mathrm{c}} = \mathbf{Z}^{\mathrm{B}}\mathbf{V}^{\mathrm{c}}. \tag{10}$$

Therefore, the impedance matrix $\mathbf{Z}^{\mathrm{B}}$ of subdomain B can be characterized by

$$\mathbf{Z}^{\mathrm{B}} = \mathbf{P}^{\mathrm{c}}(\mathbf{V}^{\mathrm{c}})^{-1} \tag{11}$$

and experiments performed only on the whole system.
However, attention must be given to the fact that this approach relies on the special case represented by Eq. (4) where no source is considered in the subdomain to be characterized.

## 3. Proof of concept of subdomain characterization

Let us consider the simple system presented in Fig. 2. It consists of a rectangular box with rigid walls having dimensions $L_x$, $L_y$ and $L_z$. This box is divided virtually into two subdomains: A and B ($\Omega = \Omega_{\mathrm{A}} \cup \Omega_{\mathrm{B}}$) coupled through the coupling surface $\Gamma$ at $x = 0.5$ m. This coupling surface is divided in this simple test case into only two square patches of the same dimension 0.2×0.2 m as presented in Fig. 2(b). The characteristics of the whole system and of subdomains A and B are listed in Table 1.

For the $k$-th experiment and according to section 2.3, the coupling pres-

| | Whole system | Subdomain A | Subdomain B |
|---|---|---|---|
| ($L_x$; $L_y$; $L_z$) [m] | (0.8; 0.4; 0.2) | (0.3; 0.4; 0.2) | (0.5; 0.4; 0.2) |
| $\rho$ [kgm$^{-3}$] | 1.29 | | |
| c [ms$^{-1}$] | 340 | | |
| $\eta$ [-] | 0.01 | | |

Table 1: Characteristics of the whole simple system and the subdomains A and B. $\rho$, $c$ and $\eta$ are the density of air, the sound speed and the damping ratio, respectively.

sures and coupling acoustic velocities are linked by Eq. (8). In this case, no source acts in subdomain B and $\mathbf{p}_k^{\mathrm{coupl}}$ and $\mathbf{v}_k^{\mathrm{coupl}}$ are quantities averaged on the surface of the patches. In this case of two patches, only two different experiments are required. An experiment consists of the "measurement" of the averaged pressures and particle velocities on the surface of the patches for two different positions of the source. In the present case, the positions of the source are located in subdomain A at (0.6; 0.05; 0.13) m and (0.7; 0.35; 0.08) m in the global coordinate system.
With these two experiments, matrices $\mathbf{P}^c$ and $\mathbf{V}^c$ (of size 2×2) can be built and Eq. (11) can be applied to retrieve the complete acoustic impedance

matrix (including off-diagonal terms) of subdomain B. The terms $Z_{ij}$ of the identified matrix are compared to a reference solution based on modal summation as described in [9] (some details can be found in AppendixA). The comparison is shown in Fig. 3.

As can be seen in Fig. 3, the proposed approach is able to efficiently predict the surface impedance of a subdomain measuring data only in the whole system when the sources are successively acting outside the subdomain under investigation. This is a remarkable property as the identified curves shown in Fig. 3 present several peaks that do not correspond to the natural frequencies of the whole system but to the natural frequencies of the subdomain B with rigid walls.
Some discrepancies appear above the $\lambda/2$ criterion for which the length of the patches (here 0.2 m) is larger than half of the acoustic wavelength $\lambda$. This frequency limit occurs in the present case at 850 Hz. This corresponds to the criterion stated by Ouisse *et al.* for the application of the PTF method [9] and by Forget *et al.* for the application of the inverse PTF method [14].
Finally, the pressure at point $M$ (see Fig. 2) can be computed using the PTF approach and the identified impedance matrix $\mathbf{Z}^{\mathrm{B,id}}$ of the passive subdomain B using Eqs. (7) and (2) even if the excitation of the active subdomain A is different from those used to identify the impedance matrix. This pressure can be compared to the one obtained by the PTF approach using the reference impedance matrix $\mathbf{Z}^{\mathrm{B,ref}}$ (obtained by modal summation, see AppendixA for more details). Ultimately, these pressures can also be compared to that obtained using a classical modal summation on the whole cavity volume $\Omega$ (see AppendixA for more details). This last comparison allows distinguishing errors due to the identification process to those due to the PTF approach itself.
In Fig. 4, the pressure at listening point (0.72; 0.28; 0.15) m when a point source is acting at (0.75; 0.06; 0.07) m is computed with the three approaches. As can be seen in Fig. 4, the three curves (reference, PTF with identified impedance matrix and PTF with reference matrices) are almost superimposed, demonstrating that the slight discrepancies on the identified impedance matrix $\mathbf{Z}^{\mathrm{B}}$ observed in Fig. 3 have rather no influence on the quality of the results. In addition, the PTF approach with the identified impedance matrix obeys the same "$\lambda/2$" criterion as that using the reference impedance matrix. This result clearly validates the proof of concept of the identification method proposed to characterize a passive vibro-acoustic subdomain.

## 4. Conditioning issues and regularization

*4.1. Errors due to ill-conditioning*

Although the proof of concept shows that the proposed identification method is capable of performing efficiently, it is obviously not free of errors. Like many inverse methods, the proposed process can be ill-posed as the condition number can reach high values at certain frequencies, as shown in Fig. 5(a). The condition number of a matrix $\mathbf{A}$ measures how much the output value $\mathbf{b}$ of a system of equations $\mathbf{Ax} = \mathbf{b}$ can change for a small change in the input vector $\mathbf{x}$. A problem with a low condition number is said to be well-conditioned, while a problem with a high condition number is said to be ill-conditioned [15]. A high value of the condition number can then indicate at which frequencies inversion problem might occur, without it being possible to define a threshold.
The curve of Fig. 5(a) exhibits peaks of condition number coinciding with the natural frequencies of the whole system (green square symbols) and the natural frequencies of passive subdomain B (red triangle symbol). Indeed,

- at the resonance frequencies of the whole system, the position of the source has little impact on the pressure distribution on the coupling surface. At these frequencies, this distribution is mostly driven by the mode shape of the resonant mode. In this case, each position of the source leads to almost the same pressure distribution on the coupling surface, causing the condition number to increase considerably.

- at the resonance frequencies of subdomain B (with rigid walls), a form of "anti-resonance" occurs in subdomain A. Subdomain A somehow acts as a blocked surface on subdomain B. At these frequencies the velocity is low in subdomain A, thereby increasing the condition number.

Conversely, the natural frequencies of the active subdomain A with rigid walls do not appear to have any influence on the condition number.
The Mean Quadratic Error (MQE) between the identified and the reference impedance matrices is defined as

$$\mathrm{MQE}(\omega) = \frac{1}{N^2} \sum_{i=1}^{N} \sum_{j=1}^{N} |Z_{ij}^{\mathrm{B,id}}(\omega) - Z_{ij}^{\mathrm{B,ref}}(\omega)|^2, \tag{12}$$

where $Z_{ij}^{\mathrm{B,id}}(\omega)$ and $Z_{i,j}^{\mathrm{B,ref}}(\omega)$ are the $(i, j)$ elements of the identified and the reference matrices $\mathbf{Z}^{\mathrm{B}}$, respectively, at the angular frequency $\omega$. It is worth

noting that the Mean Quadratic Error shown in Fig. 5(b) is affected only by the natural frequencies of subdomain B with rigid walls. Indeed, it can be seen that the mean quadratic error is low for the natural frequencies of the whole system which do not coincide with those of subdomain B. The mean quadratic error is only significant at the resonance frequencies of the subdomain under investigation (the passive subdomain).

### *4.2. Regularization effects of the median of the experiments*

When solving Eq. (10), two difficulties can occur. The first is associated with the singularity of matrix $\mathbf{V}^{\mathrm{c}}$ to be inverted. This can be due to non-independent experiments used to build the matrix, that is to say, the use of different points of excitation. Of course, using different but overly close excitation points leads to bad inversion and polluted results.

The second difficulty appears when a term of the impedance matrix has a negligible influence on the pressure and velocity field produced by the different excitations to build the matrix equation (10). In this situation, a considerable uncertainty appears on the matrix term of negligible influence, producing an ill-posed problem and a polluted result.

To solve ill-conditioned problems the standard approach is to use an a-priori regularization technique based for example on the standard Tikhonov and L-curve approaches [16]. Here we explore an a-posteriori technique, based on the observation that situations producing ill-conditioned problems are particular. Therefore, when observing several different identified impedance matrices, namely several solutions obtained from different sets of experiments, the solution observed most is the right one.

Consequently, the technique proposed to identify an impedance matrix of rank $N$ consists in solving the problem without any regularization for $P$ sets of the $N$ experiments necessary to build the matrices. Thus, an ensemble of $P$ identified impedance matrices is obtained. The regularization is performed by computing the median of the $P$ results. This a-posteriori regularization technique is very easy and straightforward to implement.

In the proof of concept described in Sec. 3, two successive experiments ($N = 2$) and thus two different positions of the source are needed. Applying Eq. (11) yields an identified impedance matrix $\mathbf{Z}^{\mathrm{B,id}}$. By changing the positions of the two sources to obtain another set of two experiments and again applying Eq. (11) yields a slightly different version of $\mathbf{Z}^{\mathrm{B,id}}$. This process can be reproduced $P$ times to obtain $P$ versions of the impedance matrix $\mathbf{Z}^{\mathrm{B,id}}$.

| Source setup 1 | | Source setup 2 | |
|---|---|---|---|
| Source ID | Coordinates [m] | Source ID | Coordinates [m] |
| $S_1^1$ | (0.76; 0.28; 0.14) | $S_1^2$ | (0.62; 0.34; 0.14) |
| $S_2^1$ | (0.74; 0.34; 0.04) | $S_2^2$ | (0.68; 0.36; 0.08) |
| $S_3^1$ | (0.72; 0.38; 0.08) | $S_3^2$ | (0.72; 0.22; 0.10) |
| $S_4^1$ | (0.74; 0.18; 0.08) | $S_4^2$ | (0.68; 0.20; 0.04) |
| $S_5^1$ | (0.62; 0.12; 0.08) | $S_5^2$ | (0.66; 0.20; 0.14) |
| $S_6^1$ | (0.68; 0.3; 0.12) | $S_6^2$ | (0.68;0.22; 0.04) |

Table 2: Source positions for two different source setups.

To regularize this inverse problem, one solution would be to average the $P$ versions of the impedance matrices $\mathbf{Z}_p^{\mathrm{B,id}}$ ($p \in [1...P]$) obtained with the $P$ sets of $N$ experiments.
In the following, $P = 15$ sets of $N = 2$ experiments (one experiment=one position of the source) are used to identify 15 versions of the impedance matrix $\mathbf{Z}_p^{\mathrm{B,id}}$. $P$ different configurations can be obtained arranging $N$ source positions among $L$ possible positions. In that case, $P$ is given by

$$P = \frac{L!}{N!(L-N)!} \tag{13}$$

where $\bullet!$ stands for the factorial of $\bullet$. Considering the $L = 6$ possible positions of the source of setup 1 described in Table 2, there are $P = 15$ different combinations of $N = 2$ different source positions. Therefore, only 6 source positions can lead to the identification of 15 different versions of $\mathbf{Z}^{\mathrm{B,id}}$.

The average of the $P = 15$ versions of the identified impedance matrix is plotted in Fig. 6(a-b). As can be seen, although several discrepancies appear at low frequency (mostly around 180 Hz and 400 Hz), the results are satisfactory in amplitude as well as in phase. This is definitely not the case when considering the $L = 6$ source positions of setup 2 described in Table 2. By changing only the $L = 6$ source positions of the setup, the quality of the results is changed dramatically. Indeed, in the case of setup 2 the results are simply not reliable. In fact, in the $P = 15$ versions of the impedance matrix, we are faced with an inversion problem (no regularization is done here). Taking the mean of the $P = 15$ versions of the impedance matrices then leads to an erroneous estimation of the matrix. The presence of only one outlier in the $P = 15$ versions (here due to the inversion problem) causes the mean to be ill-adapted to the process described to avoid classical regularization. This

problem is even more important considering the fact that no rule was found to explain the poor results obtained when using setup 2. Indeed, positions of sources in setup 2 are not so different from those of setup 1. This sensitivity to source positions makes the use of the mean not reliable.
The median of the identified impedance matrices can be used to avoid the problems encountered with the use of the mean. The results obtained with the median of the matrices are presented in Fig. 6(c-d). Contrary to the results obtained with the mean, the estimation of the impedance matrix $\mathbf{Z}^{\mathrm{B,id}}$ is very close to the reference computation whatever the source setup. This demonstrates the stability of the median regarding the possible presence of outliers in the $P$ versions of the identified impedance matrix. In addition, the discrepancies that appear at low frequency (180 Hz and 400 Hz) are completely removed when using the median instead of the mean. It is noteworthy that the mean and the median are obviously applied here to the same population of impedance matrices.

## 5. Experimental validation

In this section, the first experiment is performed to characterize the surface impedance of a rectangular box open on a "quiet" room, as shown in Fig. 7. The coupling surface between the box and the room is divided into 20 rectangular patches of size $0.164 \times 0.152$ m. The rectangular box has dimensions $L_x = 0.82$ m, $L_y = 0.608$ m and $L_z = 0.53$ m. Compared to the "proof of concept" case, this application:

- deals with many more patches (20 versus 2). In this case, the dimension of the impedance matrix to be identified is $20\times20$ for each frequency under investigation. The minimal number of source positions is thus 20. In the following, 25 source positions are used (see Fig. 7(b)) to create $P = 53130$ sets of $N = 20$ experiments (Eq. 13).

- implies the presence of background noise on the measurement of pressure and velocity on patches.

- implies replacing the integral of the spatial average of pressure and velocity on the surface of the patches by the value of pressure and velocity at the center of the patches. This approximation is valid when the size of the patches is small compared to the wavelength.

From the practical viewpoint, pressure and particle velocity at the center of each patch are measured by an array of 20 PU probes (Microflowns sensors able to measure pressure and particle velocity, see Fig. 7(a)) for each of the $L = 25$ source positions described in Fig. 7(b). The source positions are obviously outside the subdomain (the box) to be characterized. The low frequency monopole sound source was a *LMS Qsources* device fed with a white noise. The omni-directionality frequency range of this source is [20:2000] Hz. However, one has to notice here that any type of source might be used for this experiment and a monopole source is not mandatory. The measurements were performed in the [0:1000] Hz frequency band. In this frequency band, the proposed approach should be reliable considering the size of the patches and the $\lambda/2$ criterion stated previously.
The results of the identification process using the median on 21 over the $P = 53130$ possible combinations of $N = 20$ source positions are presented in Fig. 8 for components $Z^{B,\mathrm{id}}_{1,1}$ and $Z^{B,\mathrm{id}}_{3,16}$ of the impedance matrix. The amplitude as a function of frequency of these two components is compared to a reference analytic computation assuming a rectangular idealized box filled with air with a sound speed of $c_0 = 340$ ms$^{-1}$, a density $\rho_0 = 1.29$ kgm$^{-3}$ and a damping $\eta_0 = 0.01$ (see AppendixA for more details). The chosen parameters are usual ones without any tuning. Especially, damping was not measured and a constant value was chosen.
As can be seen in Fig. 8, the identification process is able to characterize the surface impedance of a passive acoustic subdomain without uncoupling it from the whole system and without classical regularization of the inversion of the matrix $\mathbf{V}^{\mathrm{c}}$. However, two comments are needed: (i) PU probes are not designed to measure pressure and particle velocity below 100 Hz. Below this frequency, the coherence between signals was poor and the results are thus unreliable. (ii) The damping of the air cavity seems higher than the one used in computations (some peaks are smoother on the identified curve than on the computed one). However, the damping parameter was already chosen quite high. This might point out that the process of the proposed approach has a smoothing effect on the results even if this was not noticed in numerical simulations. This aspect will be investigated in further experiments.

## 6. Conclusion

In this article, an experimental characterization of the surface impedance of a passive acoustic (or vibro-acoustic) subdomain was proposed. It is based

on the Patch Transfer Functions (PTF) formulation and an inverse approach. A proof of concept demonstrated that this approach is able to estimate the complete "patch-to-patch" surface impedance matrix of the passive subdomain without uncoupling it from the whole system. The quality of the results was limited by the $\lambda/2$ criterion as observed previously in the literature for the PTF approach. Since the impedance matrix is intrinsically independent of the coupling, the subdomain characterized can be then used in any numerical simulation to test different configurations.
The proposed approach is theoretically applicable to both acoustic and vibroacoustic subdomains of any shape. However, as this approach characterizes only surface impedance, the subdomain must be passive (no source inside). The initial experimental validation was performed and demonstrated that the approach proposed gives satisfactory results in real conditions.

**Acknowledgements**

This work was performed within the framework of the LABEX CeLyA (ANR-10-LABX- 0060) of Université de Lyon, within the program "Investissements d'Avenir" (ANR-16-IDEX-0005) operated by the French National Research Agency (ANR).
This study was financed by the BMW Group and performed in collaboration with the "Laboratoire Vibrations Acoustique" of the INSA-Lyon engineering school.

## AppendixA. Reference computation for a rectangular box

Let us consider a rectangular box (dimensions $L_x \times L_y \times L_z$) with rigid walls filled with air (sound speed $c_0$, density $\rho_0$ and damping factor $\eta_0$). A unit acoustic point source is active in the cavity at point $Q$. Pressure $p(M,\omega)$ at angular frequency $\omega$ can be expressed on the basis of mode shapes $\phi_n(M)$ as

$$p(M,\omega) = c_0^2 \sum_{m=1}^{\infty}\sum_{n=1}^{\infty}\sum_{p=1}^{\infty} \frac{\phi_{mnp}(M)\phi_{mnp}(Q)}{(\omega^2 - \omega_{mnp}^2 + \ \mathrm{i}\eta_0\omega\omega_{mnp})\Lambda_{mnp}} \tag{A.1}$$

where $\Lambda_{mnp}$ is the norm of mode of indices $(m,n,p)$. The mode shape $\phi_{mnp}(M)$ ($M$ being a point of coordinates $(x,y,z)$) is given by

$$\phi_{mnp}(x,y,z) = cos\left(\frac{m\pi}{L_x}x\right) cos\left(\frac{n\pi}{L_y}y\right) cos\left(\frac{p\pi}{L_z}z\right) \tag{A.2}$$

and the angular Eigen-frequency is given by

$$\omega_{mnp} = c_0 \sqrt{\left(\frac{m\pi}{L_x}\right)^2 + \left(\frac{n\pi}{L_y}\right)^2 + \left(\frac{p\pi}{L_z}\right)^2}. \tag{A.3}$$

The norm $\Lambda_{mnp}$ is given by

$$\Lambda_{mnp} = \frac{L_x L_y L_z}{8} 2^d \tag{A.4}$$

where $d$ is the number of null indices among $m$, $n$ and $p$.
The surface impedance between a patch $i$ and a patch $j$ is given by [9]

$$Z_{ij}(\omega) = \mathrm{i}\omega\rho_0 c_0^2 \sum_{m=1}\sum_{n=1}\sum_{p=1}^{\infty} \frac{\langle \phi_{mnp}(L)\rangle_{L\in\Gamma_i} \langle \phi_{mnp}(N)\rangle_{N\in\Gamma_j} \Gamma_j}{(\omega^2 - \omega_{mnp}^2 + \mathrm{i}\eta_0\omega\omega_{mnp})\Lambda_{mnp}} \tag{A.5}$$

where $\langle \phi_{mnp}(L)\rangle_{L\in\Gamma_i}$ denotes the spatial average of mode shape $\phi_{mnp}(L)$ on the patch surface $\Gamma_i$.


[1] D. de Klerk, D. J. Rixen, S. N. Voormeeren, General Framework for Dynamic Substructuring: History, Review, and Classification of Techniques, AIAA J., vol. 46(5) (2008) 1169-1181.

[2] P. Gardonio, M. J. Brennan, On the origins and development of mobility and impedance methods in structural dynamics, J. Sound. Vib. 249(3) (2002) 557-573.

[3] M. V. van der Seijs, D. de Klerk, D. J. Rixen, General Framework for Transfer Path Analysis: History, Theory and Classification of Techniques, Mech. Syst. Signal Process. 68-69 (2016) 217-244.

[4] C. Cacciolati, J.-L. Guyader, Acoustic mobility for vibroacoustic prediction, in Proceedings of ICSV 7, Garmisch-Partenkirchen, Germany, 2000.

[5] J.-D. Chazot, J.-L. Guyader, Prediction of transmission loss of double panels with a patch-mobility method, J. Acoust. Soc. Am. 121(1) (2006) 267-278.

[6] J.-D. Chazot, J.-L. Guyader, Transmission loss of double panels filled with porogranular materials, J. Acoust. Soc. Am. 126 (2009) 3040-3048.

[7] J.-L. Guyader, C. Cacciolati, J. D. Chazot, Transmission loss prediction of double panels filled with porous materials and mechanical stiffeners, in Proceedings of ICA, Sydney, Australia, 2010.

[8] L. Maxit, C. Cacciolati, J.-L. Guyader, Airborne noise prediction using patch acoustic impedance, in Proceedings of ICSV 9, Orlando, USA, 2002.

[9] M. Ouisse, L. Maxit, C. Cacciolati, J.L. Guyader, Patch Transfer Functions as a Tool to Couple Linear Acoustic Problems, J. Vib. Acoust. 127(5) (2005) 458-466.

[10] N. Totaro, J.L. Guyader, Efficient positioning of absorbing material in complex systems by using the Patch Transfer Functions method, J. Sound. Vib. 331 (2012) 3130-3143.

[11] J. Rejlek, G. Veronesi, C. Albert, E. Nijman, A. Bocquillet, A Combined Computational-Experimental Approach for Modelling of Coupled Vibro-Acoustic Problems, SAE International, 2013.

[12] L. Du, Characterisation of Air-borne Sound Sources using Surface Coupling Techniques, PhD dissertation, Institut National des Sciences Appliquées de Lyon, Villeurbanne, France, 2016.

[13] G. Veronesi, A novel PTF-based experimental characterisation for poroelastic liners: Method and sampling criterion, PhD dissertation, Università degli Studi di Ferrara, Ferrara, Italy, 2015.

[14] S. Forget, N. Totaro, J.L. Guyader, M. Schaeffer, Source fields reconstruction with 3D mapping by means of the virtual acoustic volume concept, J. Sound. Vib. 381 (2016) 48-64.

[15] C. Hansen, Rank-deficient and discrete ill-posed problems: numerical aspects of linear inversion, Society for Industrial and Applied Mathematics, 1998.

[16] N. Totaro, D. Vigoureux, Q. Leclère, J. Lagneaux, J.-L. Guyader, Sound fields separation and reconstruction of irregularly shaped sources, J. Sound. Vib. 336 (2015) 62-81.

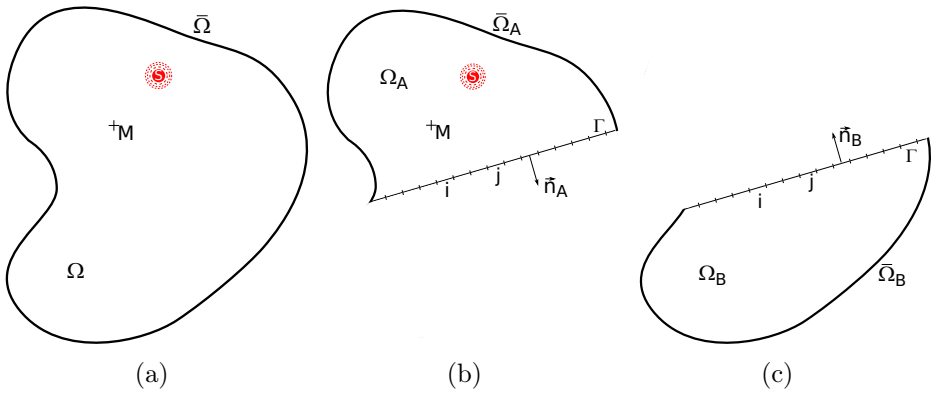


Figure 1: (a) the whole system $\Omega$ under study excited by an acoustic source S and delimited by a boundary surface $\partial\Omega$ (here considered as rigid); (b) subdomain A delimited by surfaces $\partial\Omega_A \cup \Gamma$; (c) subdomain B delimited by surfaces $\partial\Omega_B \cup \Gamma$. $\vec{n}_A$ and $\vec{n}_B$ are respectively the outward normals of subdomains A and B. The coupling surface $\Gamma$ is divided into patches referenced by indices $i$ and $j$.

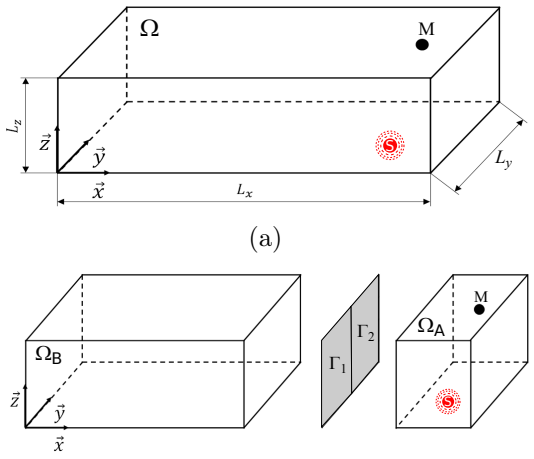


Figure 2: (a) the whole system Ω under study excited by an acoustic source S; (b) subdomains A and B coupled through the coupling surface Γ divided into 2 square patches.

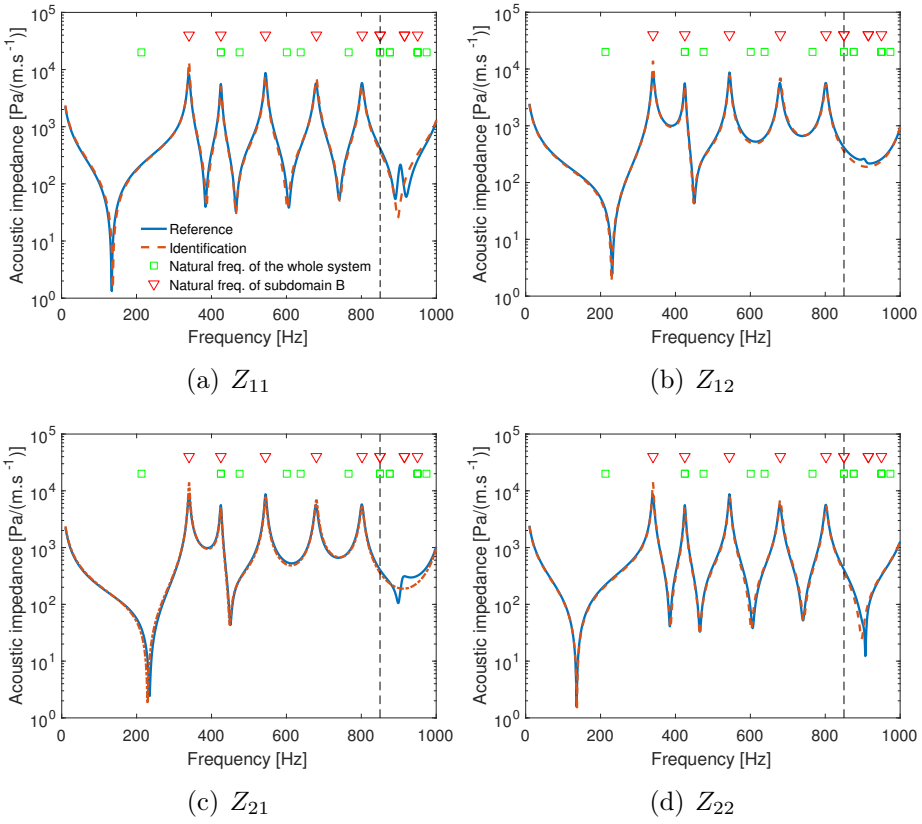


(a) $Z_{11}$ (b) $Z_{12}$

(c) $Z_{21}$ (d) $Z_{22}$

Figure 3: Amplitudes of terms $Z_{ij}$ of the reference matrix (solid lines) and of the matrix identified (dashed-dotted lines) as a function of frequency. (a) $Z_{11}$; (b) $Z_{12}$; (c) $Z_{21}$; (d) $Z_{22}$. The vertical dashed line represents the "$\lambda/2$" criterion. $\square$: positions of the natural frequencies of the whole system; $\triangledown$: positions of the natural frequencies of the subdomain B with rigid walls.

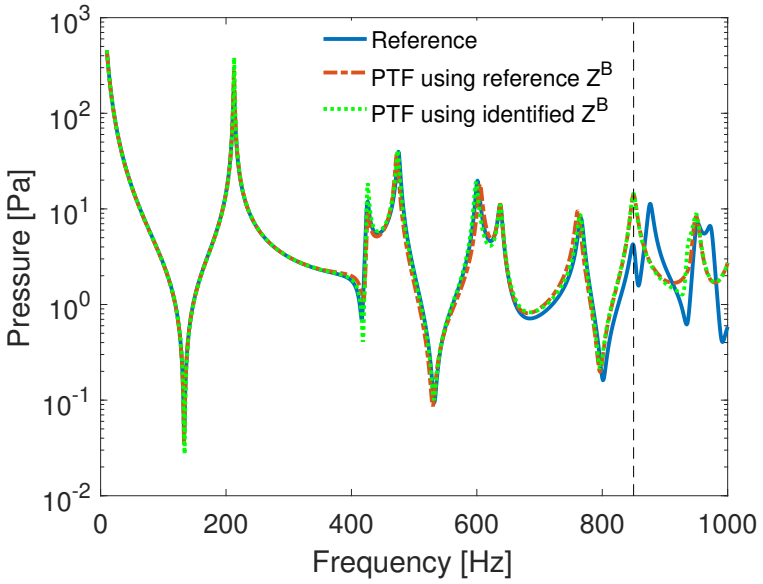


Figure 4: Pressure at point M as a function of frequency. Solid line: reference computation; dashed line: PTF computation using reference impendance matrices; dotted line: PTF computation using identified impedance matrices. The vertical dashed line represents the "$\lambda/2$" criterion.

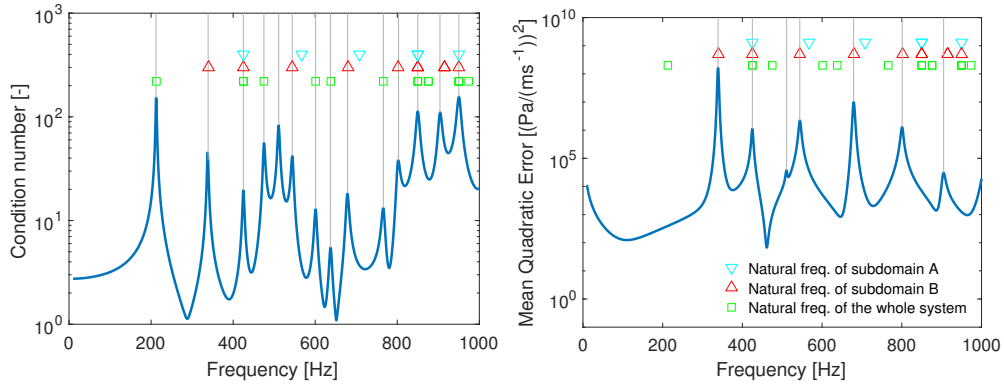


(a) (b)

Figure 5: (a) Condition number of the velocity matrix $\mathbf{V}^c$ as a function of frequency; (b) Mean Quadratic Error between the identified and the reference matrices as a function of frequency. $\square$: positions of the natural frequencies of the whole system; $\triangledown$: positions of the natural frequencies of the active subdomain A with rigid walls; $\triangle$: positions of the natural frequencies of the passive subdomain B with rigid walls.

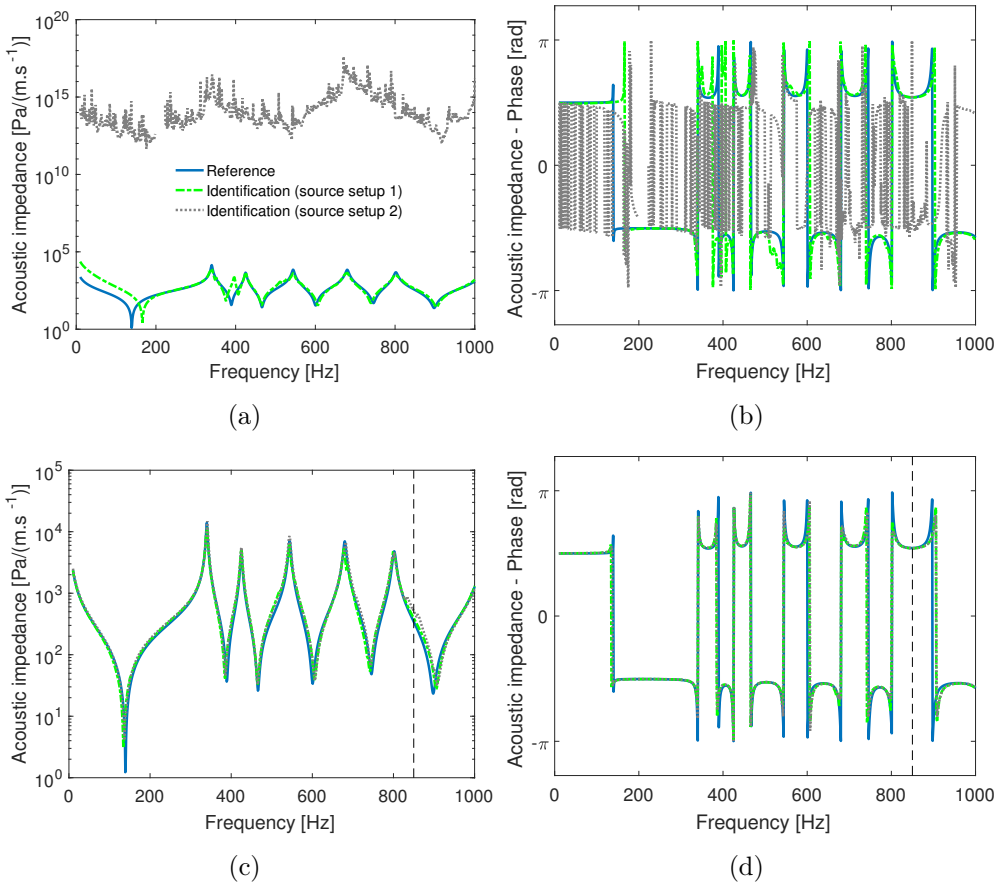


Figure 6: (a) amplitude and (b) phase of the component $Z_{11}^{B,\mathrm{id}}$ obtained averaging the $P = 15$ versions of the impedance matrix $\mathbf{Z}^{\mathrm{B,id}}$. (c) amplitude and (d) phase of the component $Z_{1,1}^{B,\mathrm{id}}$ obtained taking the median of the $P = 15$ versions of the impedance matrix $\mathbf{Z}^{\mathrm{B,id}}$. Solid curve: reference computation; dashed-dotted line: using source setup 1; dotted line: using source setup 2.

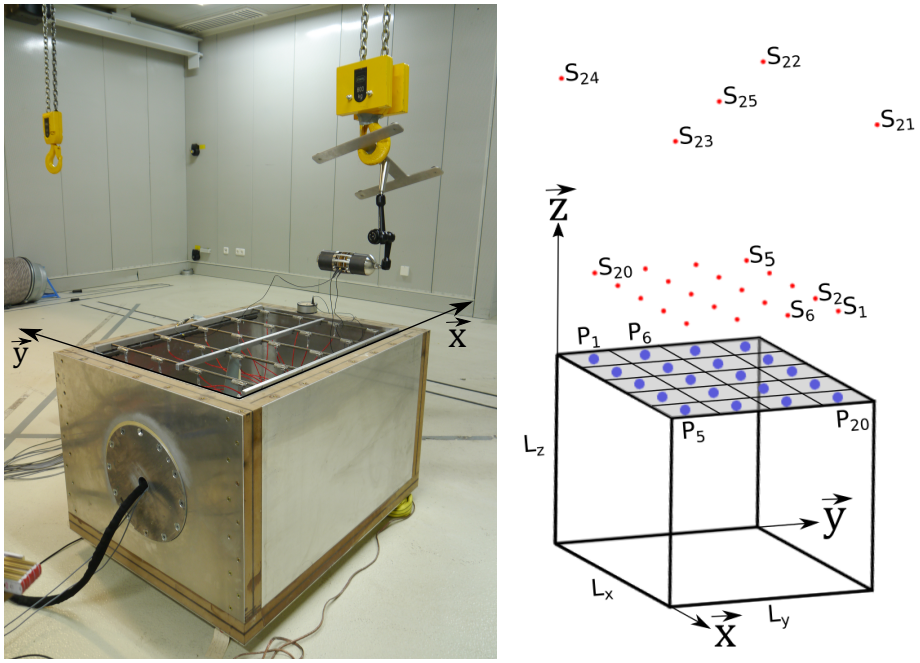


(a) (b)

Figure 7: (a) Picture of the subdomain (the box) to characterize coupled to a large "quiet" room. The pressure and particle velocity at center of each patch are measured using an array of 20 PU probes. The point source is moved at 25 different positions. (b) Sketch of the patches, the positions of the centers of $N = 20$ patches and the positions of the $L = 25$ sources.

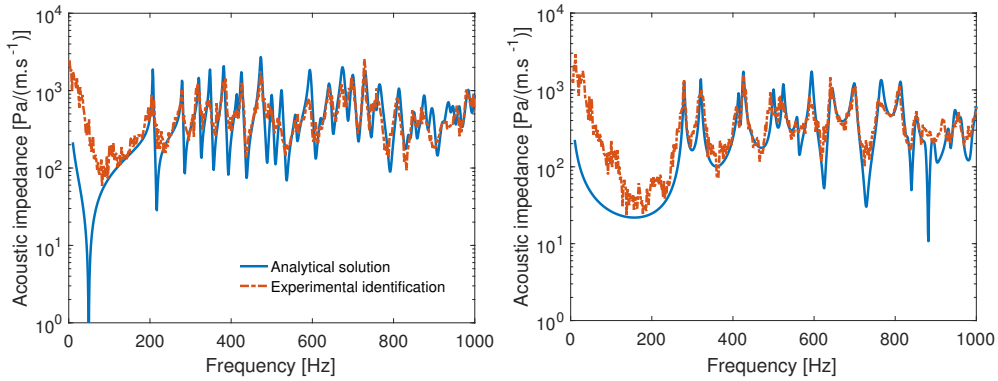


Figure 8: Comparison of impedances obtained from experimental identification and from an analytic solution. (a) $Z^B_{1,1}$ (b) $Z^B_{3,16}$. Solid line: reference analytical solution; dashed-dotted line: experimental identification.